JOURNAL OF MATERIALS SCIENCE 29 (1994) 2968–2980

The relevance of the surface structure and surface chemistry of carbon fibres in their adhesion to high-temperature thermoplastics

Part I *Surface structure and morphology*

G. KREKEL, K. J. HÜTTINGER
Institut für Chemische Technik, Universität Karlsruhe, Kaiserstrasse 12, D-7500 Karlsruhe, Germany

W. P. HOFFMAN, D. S. SILVER
Phillips Laboratory, OLAC PL/RKFE Edwards Air Force Base, Edwards, CA, 93523-5000, USA

The surface structure and morphology of several high strength polyacrylonitrile (PAN) based carbon fibres was studied with the scanning electron microscope (SEM) on the micrometre scale and the scanning tunnelling microscope (STM) down to the atomic scale. In addition, active surface area measurements were made to determine the number of bonding sites/unit area. Prior to the observations, the surfaces of some of the samples were subjected to either the commercial surface treatment or to oxidation in air or ozone in our laboratory. The roughness and number of bonding sites on each fibre surface was determined. These values will be correlated with the mechanical properties of composites made with these fibres and thermoplastic polymers in Part III of this study.

1. Introduction

Carbon-fibre-reinforced polymers are used in many fields, but they are principally employed as structural materials in the aerospace industry [1–2]. In spite of the fact that these composites are commercial products, many aspects of these materials are not yet clearly understood. One of the remaining fundamental questions concerns the adhesion of the polymer matrix at the carbon-fibre surface. The optimum use of the reinforcement properties of carbon fibres is only possible in the case of maximum adhesion.

In general, adhesion results from different interactions across the interface [3–5]; these interactions include: dispersive interactions (London Forces), non-dispersive interactions based on acid–base interactions, and covalent chemical bonds. These physico-chemical interactions can be strongly enhanced by mechanical interlockings.

Adhesion phenomena are not only complex, but from a scientific point of view they are also not yet completely understood. The reasons are as follows.

1. The surface of the carbon fibres is complex with respect to their structure and to their chemistry.

2. Many thermosetting resins are two-component systems. During curing, both components can interact or react with the functional groups at the carbon-fibre surface in different ways.

3. Thermoplastic polymers can specifically interact with the fibre surface only through their functional groups. However, the orientation of the functional groups with respect to the fibre surface has not yet been experimentally studied.

4. The current scientific understanding of the interactions across the interface and their experimental analysis is insufficient.

The extraordinary properties of carbon fibres are a consequence of the anisotropic graphite lattice. High strength (HT) fibres enjoy the greatest commercial use and for this reason they were used in the present study. The structure of carbon fibres has been investigated in the past mainly to correlate with the mechanical properties [6–8]. The preferred analytical methods have been X-ray diffraction (XRD) techniques [9, 10] and high-resolution electron microscopy (HREM) [9, 11–13] as well as scanning electron microscopy (SEM) and polarized-light microscopy [10, 14]. Typical fibre cross-sections [15] are shown in Fig. 1. Using only these techniques, the information obtained concerning the atomic structure of the outer layers of the fibre surface and their orientation with respect to the surface is incomplete [4, 16–17]. On the other hand, the surface structure is of fundamental importance for the understanding of adhesion phenomena. Scanning tunnelling microscopy offers the possibility to fill this need [18–20] and will be applied along with SEM in the present study to characterize the structure of the carbon-fibre surfaces.

The surface chemistry of carbons in general, and of

0022–2461

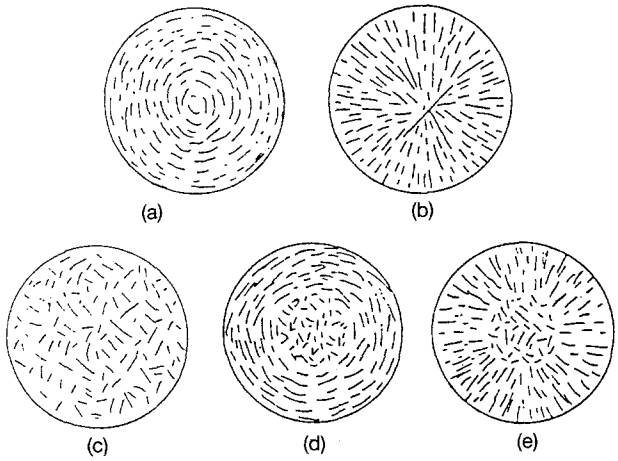

Figure 1 Typical cross-sections of carbon fibres (according to Herakowitch [15]). (a) Concentric orthotropic. (b) Radial, orthotropic. (c) Transversal, isotropic. (d) Concentric isotropic; centre, transversal, isotropic. (e) Radial, orthotropic; centre, transversal, isotropic.

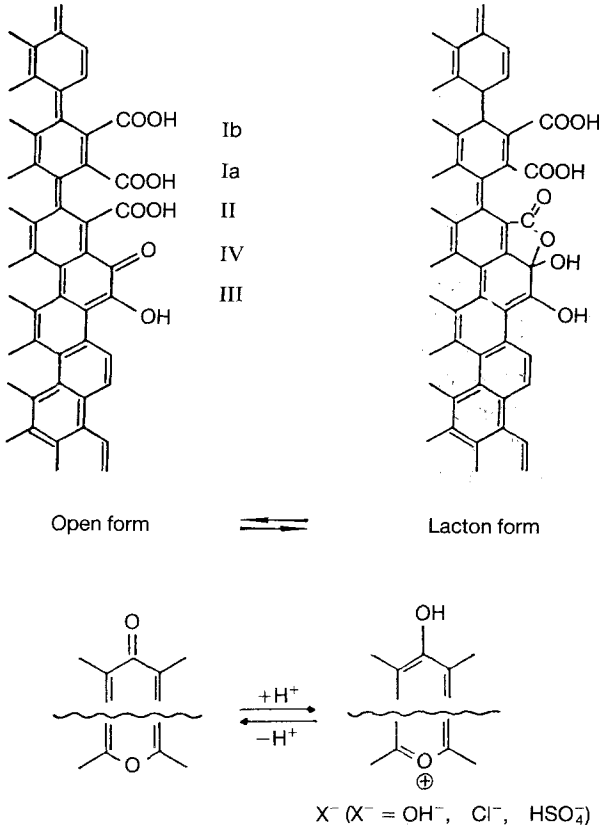

Figure 2 Possible oxygen-containing groups at carbon-fibre surfaces (according to Boehm *et al.* [22]).

carbon fibres in particular, is controlled by oxygen-containing functional groups. The present knowledge is based mainly on investigations, which were performed by Boehm and co-workers [21–25] and by other workers [26–29] in the 1960s and 1970s. Fig. 2 gives a representation of oxygen-containing surface groups according to Boehm *et al.* [22]. These surface groups consist of basic (pyrone-like structures), neutral (quinone-like structures) and acidic surface groups (carboxylic and hydroxylic groups). These acidic surface groups exhibit different acidities. Carboxylic groups may be strongly acidic (group I, neutralization with $NaHCO_3$) or weakly acidic (group II, neutralization with Na_2CO_3). Hydroxylic groups (group III) can be neutralized with NaOH and carboxylic groups can add sodium ethanolate [22–24, 30]. It is clear that the above characterizations are based on wet-chemical analysis.

More recent investigations have been performed with the aid of X-ray photoelectron spectroscopy (XPS), auger electron spectroscopy (AES), secondary-ion mass spectrometry (SIMS) and Fourier-transform infrared spectroscopy (FT-i.r.) [31–41]. These invest igations have more or less confirmed the existence of the surface groups described in the previous paragraph. In addition to wet-chemistry techniques, XPS was also used in the present study for analysis of the surface chemistry of the carbon fibres.

An important method for the determination of the quantity of the various functional groups is thermal desorption. This technique can be applied by using shock heating or a programmed temperature increase. In the latter case, the method is also known as temperature-programmed desorption (TPD). During TPD, gases such as H_2O, CO_2, CO and occasionally CH_4 and H_2, which are formed by the thermal decomposition of the surface groups, are measured. Due to the difference in thermal stability of the various functional groups, the desorption peaks of the various gases can be directly correlated to the oxygen-containing surface groups [21, 22, 25, 29, 30, 42–50]. Because of its quantitative character, TPD was also used in the present study.

An additional technique for characterizing the surface chemistry of solids makes use of wetting techniques [5, 51–56]. With the more advanced wetting techniques, dispersive and non-dispersive interactions can be differentiated [57–60]. Using these methods, the work of adhesion is calculated using the measured contact angles which are then correlated to special acid–base interactions. From these acid–base interactions, the nature and concentration of surface functional groups can be deduced. In the present study, a recently developed wetting method was applied [61–64]. In the studies of other groups [65–69] inverse gas chromatography (IGC) is used in place of wetting techniques for the same purpose. The IGC method is based on the molecular adsorption of various polar and non-polar gaseous species. It is from this adsorption that dispersive and non-dispersive interactions are to be derived. This molecular adsorption occurs on the surface as well as in the open-pore structure, and thus some information is obtained that might not be relevant to adhesion. In contrast to IGC methods, the advantage of wetting methods lies in the fact that only the interactions with the outer-most layers of the solid surface are measured. In the present study, advanced wetting techniques [61–64] were also used to characterize polymer surfaces.

In regard to polymers for matrices, thermosetting epoxy resins currently enjoy the dominant position. For this reason, it is not surprising that the majority of the investigations concerning adhesion phenomena at

carbon-fibre surfaces were performed using these matrix systems [70–79].

From the scientific point of view, interface phenomena are extremely complex in these epoxy systems, because they represent two component systems (resin + curing agent), and thus there is the possibility of both components reacting or interacting with surface functional groups. It is for this reason, that several very different models for the interpretation of adhesion phenomena [75, 76, 80] have been developed (Fig. 3). Because of the complications, an epoxy resin was used in the present study for comparison only.

Thermoplastics, especially high-temperature thermoplastics, offer numerous advantages [81–83] over thermosetting resins as matrix materials. The most important being: high-impact strength, the possibility of thermal after-moulding and welding, no extended curing cycles, unlimited storage of prepregs and the prospect of recycling.

Examples of high-temperature thermoplastics include polycarbonate, polysulphone, polyethersulphone, polyarylsulphone, polyetherimide or nylon as amorphous thermoplastics and polyphenylenesulphide or polyetheretherketone as partially crystalline thermoplastics. In the present study polycarbonate (PC) and polyethersulphone (PES) were used. In both cases, the material consists of macromolecules with functional groups, which can undergo selective interactions with the functional groups at the carbon-fibre surface. It is for this reason, in addition to their technical attractiveness, that they were used in the present study. Another reason for using these polymers is that the adhesion in such systems has only been studied to a small extent. The main purpose of the study was to clarify whether selective interactions take place and by how much such interactions contribute to adhesion. To achieve the maximum information, these polymers were combined with carbon fibres from different producers which had been treated in various ways both by the producer and in our laboratory.

Unidirectional composites were manufactured in order to examine the conclusions from the physicochemical investigations of both the fibres and the polymers. These composites were characterized by measuring the interlaminar-shear strength and the flexural strength. In addition, the fracture surfaces of the composites were investigated with the aid of polarized-light microscopy and SEM.

This present paper is concerned with the surface structure and morphology of the carbon fibres before and after surface treatments. The results of the surface chemistry of both the fibres and the polymers will be presented in Part II. Part III deals with the reinforcement of the high-temperature thermoplastics with the various fibres and correlations of the adhesion phenomena (concluded from the results of Part I and II) with the mechanical properties of the composites.

2. Experimental procedure

2.1. Materials

The fibres used in this study were all high-strength polyacrylonitrile- (PAN) based fibres. These fibres were obtained from various manufacturers both with and without sizing and/or surface treatment. Their mechanical properties, as provided by the manufacturers, are given in Table I. The Celion and Tenax fibres were manufactured under the same licence but by a slightly different process and so should bear some similarities to one another. The Hercules fibre on the other hand used both a different precursor and a different process than either the BASF or AKZO fibre.

The argon used in this study had an as-received purity of 99.998% and was then further purified in oxysorb so that the oxygen content was less than

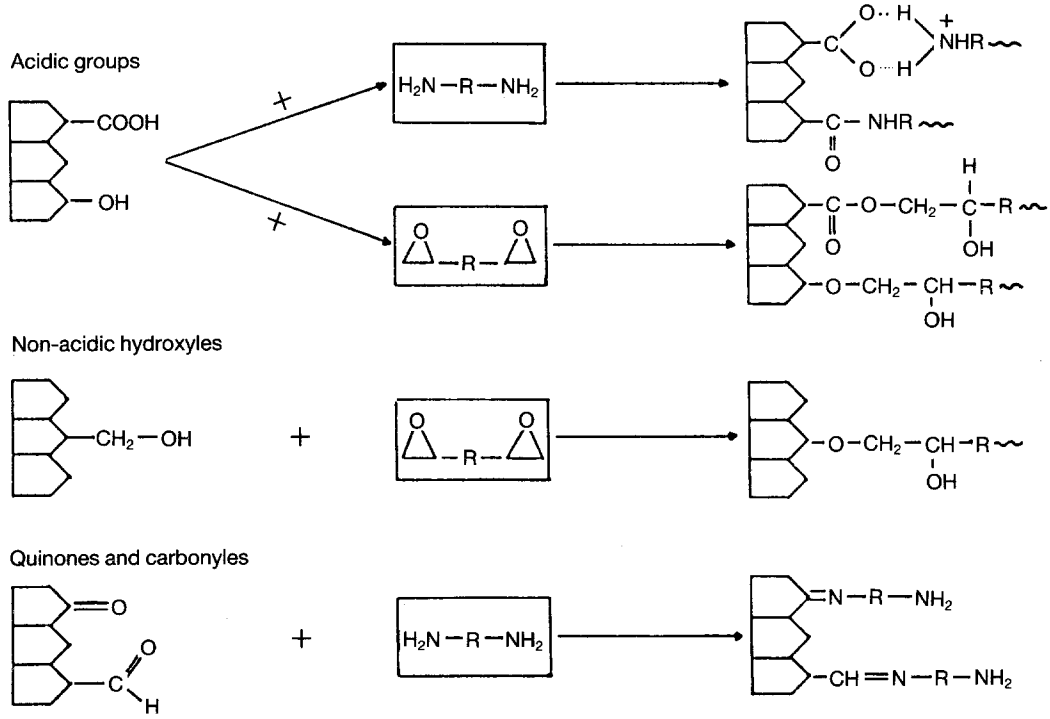

Figure 3 Possible reactions of carboxylic groups at carbon-fibre surfaces with the components of epoxy resins [75, 80].

TABLE I Selected properties of the carbon fibres used

Typical properties	Fibre		
	Celion G30-500 (BASF Celanese)[a]	Tenax HTA-7C (AKZO Faser AG)[a]	AS4 (Hercules Aerospace)[a]
Tensile strength (MPa)	3792	3840	3722
Young's modulus (GPa)	234	234	226
Strain-to-failure (%)	1.62	1.64	1.65
Weight per unit length, ($g\,m^{-1}$)	0,404[b]	0,400[b]	0,874[b]
Density ($kg\,m^{-3}$)	1780	1770	1770

[a] Producer.
[b] For 6k or 12k plies, respectively; applying surface treatments other values were measured.

0.1 p.p.m. (parts per million). The oxygen used for fibre surface treatment had a purity of 99.5% while for the chemisorption studies the oxygen had a purity of 99.995%. The krypton used for the total-surface-area determinations had a purity of 99.994%.

2.2. Apparatus and procedures

The apparatus and procedure for measuring the oxygen active surface area for carbon fibres is described elsewhere [84, 85]. The total surface area measurements employed krypton as an adsorbate and were made by a standard Brunaer–Emmett–Teller BET technique [86] using a commercial system (Micomeritics Digisorb 2600).

A Cambridge stereoscan model S4-10 scanning electron microscope was used to view the fibre surfaces in the micrometre range while a Digital Instruments nanoscope II scanning tunnelling microscope (STM) was used for submicrometre images of the fibre surfaces. The STM was operated in the constant-current mode using a tunneling current of 2–9 nA and a bias voltage of ~ 25 nV. A description of this instrument and its operation is given in [20].

For the oxygen fibre surface treatment, the fibre sample was wrapped on a carbon–carbon frame and placed in a 50 mm aluminium-oxide reactor. The tube was evacuated and flushed with oxygen before it was heated at $5\,K\,min^{-1}$ to the reaction temperature. The oxygen flowed over the fibre at $2\,l\,h^{-1}$ at various isothermal temperatures for varying periods of time.

When treating the fibre with ozone, the fibre was wrapped on an aluminium frame and held at 373 K. An ozone generator (Model GSG001.2 from Sorbios GmbH) was used to obtain 0.75% ozone in pure oxygen which was flowed at a rate of $20\,l\,h^{-1}$ around the fibre for 60 s. Table II summarizes the types of fibres used in this study, the commercial pre-treatments and the additional treatments.

3. Results

3.1. Scanning electron microscopy

3.1.1. Original fibres from different manufacturers

A comparison of the surfaces of the various industrially oxidized carbon-fibre types by SEM showed significant differences in their structures (Figs 4–6). Tenax and Celion fibres exhibited fibrillar surface structures, while the surface of the AS4 fibre was smooth and did not show any fibrils. All fibres showed contamination of the surfaces due to adhesion of small particles.

The fibrillar structure of the Tenax and Celion fibres was oriented parallel to the fibre axis. It is

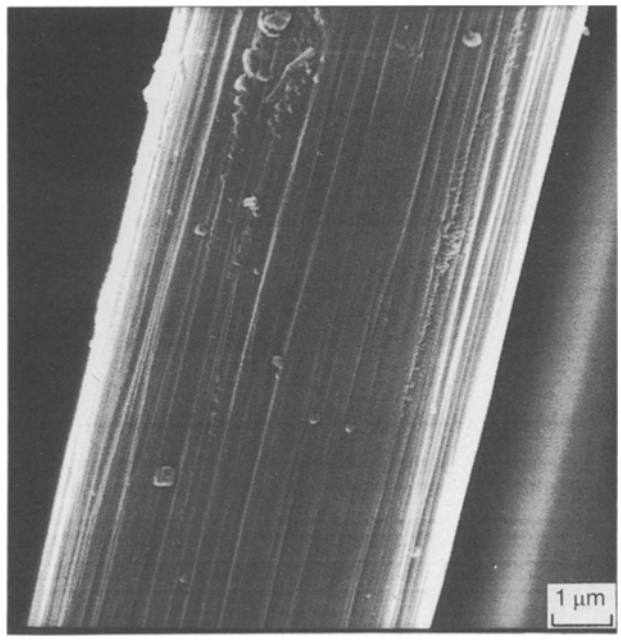

Figure 4 SEM view of the surface of a commercially oxidized, unsized Tenax fibre.

TABLE II Fibres and surface treatments applied in the present study

Type	Commercial pre-treatment	Abbreviation	Treatment
Celion	Unoxidized, unsized	Celion (uu)	None
Celion	Oxidized, unsized	Celion (ou)	None
Celion	Oxidized, sized	Celion (os)	None
Celion	Unoxidized, unsized	Celion (uu)	O_2/400 °C/0.5 h
Celion	Unoxidized, unsized	Celion (uu)	0.75%, O_3/100 °C/60 s
Tenax	Unoxidized, unsized	Tenax (uu)	None
Tenax	Oxidized, unsized	Tenax (ou)	None
AS4	Oxidized, unsized	AS4 (ou)	None

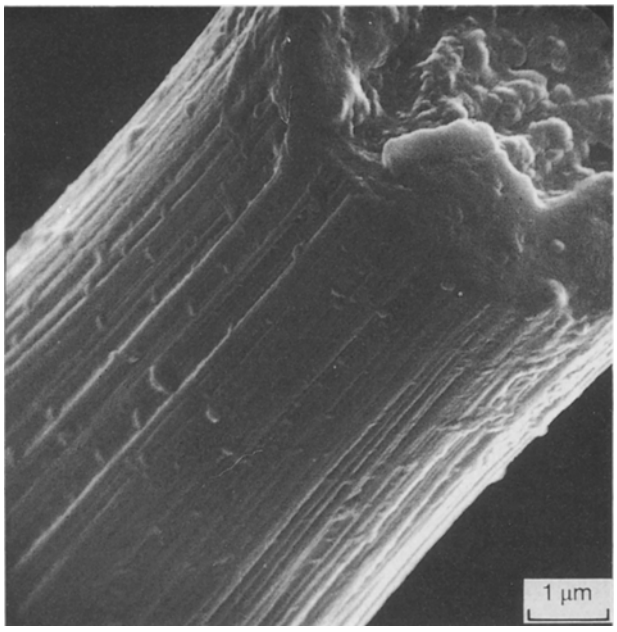

Figure 5 SEM view of the surface of a commercially oxidized, unsized Celion fibre.

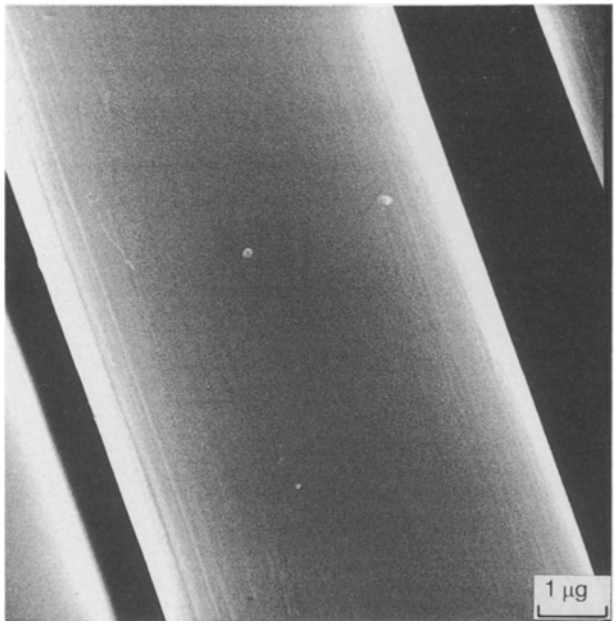

Figure 6 SEM view of the surface of a commercially oxidized, unsized, AS4 fibre.

assumed that this results in some way from the stretching of the fibrous PAN precursor. In the case of the Tenax fibres, the fibrils were extremely thin, and they were separated by deep grooves (Fig. 4). The Celion fibres had bundles of micofibrils and the grooves between the fibril bundles were relatively deep (Fig. 5). No fibrils could be detected on the surface of the AS4 fibres, due to a difference in the manufacturing process. On these fibres only some stripes in the axial direction can be seen (Fig. 6).

These results obtained with the aid of SEM demonstrate that it is possible to differentiate between the fibres at these magnifications. The AS4 fibre clearly exhibited the lowest surface roughness, when compared to the Tenax and Celion fibres. A structural differentiation is also possible with respect to the fibrils and microfibrils existing at the surface. But it is impossible to deduce from the scanning electron micrographs any information about the atomic surface structure or the orientation of the graphitic layers at the surface of the fibres.

3.1.2. Surface-treated fibres

SEM was not able to detect any changes in the surface structure of fibres exposed to either an oxidative or a thermal treatment. Thus, neither a treatment in oxygen at 400 °C for 0.5 h nor oxidation with ozone at 100 °C (0.75% O_3 for 1 min) altered the surface structure sufficiently to be discernable by SEM. For this reason, no SEM micrographs of surface-treated fibres will be shown.

3.1.3. Sized fibres

Fig. 7 shows the surface of a sized Celion fibre. It can be observed that the striations of the fibrillar structure are partly filled with sizing, but they can still be recognized. The outer regions of the fibrils also seem to be coated with the sizing agent. The microroughness of the sized fibres, compared to the unsized fibres, is increased; this mainly results from striations perpendicularly oriented to the axis of the fibre.

3.2. Scanning tunnelling microscopy

3.2.1. Celion-types

3.2.1.1. Unoxidized fibres (uu). Celion carbon fibres, like the other fibres used in this study, are produced starting with PAN as a precursor. Since the maximum heat-treatment temperature for the Celion fibres is in

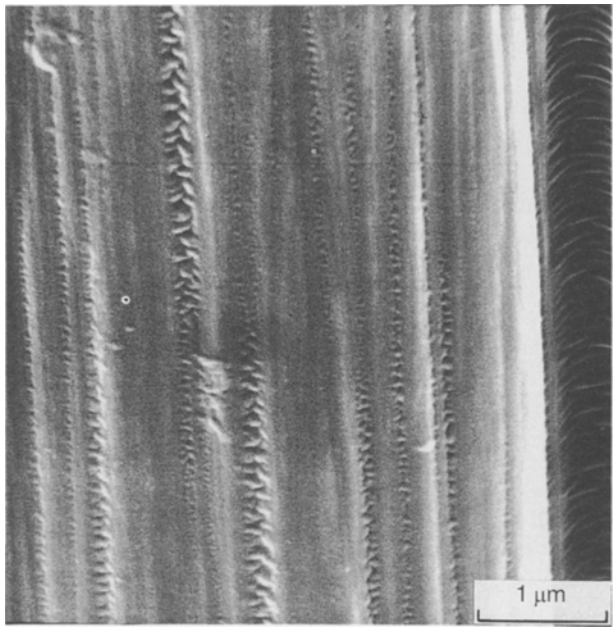

Figure 7 SEM view of the surface of a commercially oxidized, sized Celion fibre.

the range 1400 °C, these fibres still contain about 1–2 wt % hydrogen and 1 wt % nitrogen [8]. The preferred orientation of the graphitic layers along the fibre axis is a consequence of the precursor polymer, and the stretching of the virgin spun PAN fibre. Thus, the stabilization treatment is important for both a fibre's bulk properties and its surface.

Scanning tunnelling micrographs of the surface of an unoxidized Celion fibre (uu) are shown in Figs 8–11. The surface of this Celion fibre with a magnification that is about ten times greater than that obtained by SEM can be seen in Fig. 8. At this magnification, the structure and morphology of the single fibrils can be detected. A series of small holes can be observed parallel to the fibre axis. In some cases the holes are interconnected, forming elongated slits. The depth of these holes and slits is in the range 50–150 nm. At a higher magnification (Fig. 9) the surface roughness is even more pronounced. However, it should be mentioned that investigations of other parts of the surface using the same magnification also show some smoother areas, without holes. In these areas resolution down to atomic dimensions is possible. Fig. 10a shows a surface view of a non-graphitic area imaged at atomic dimensions in a rather smooth (on the submicrometre scale) region of the fibre surface. A top-view image of a similar area (Fig. 10b)

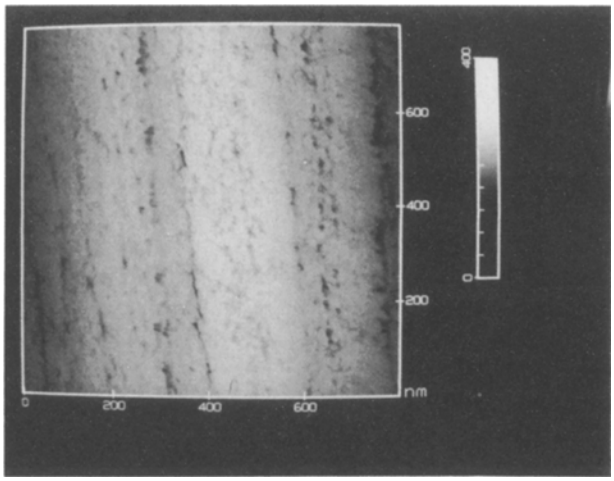

Figure 8 An 800 nm STM scan on the surface of a Celion fibre (uu) showing the pitting in the surface.

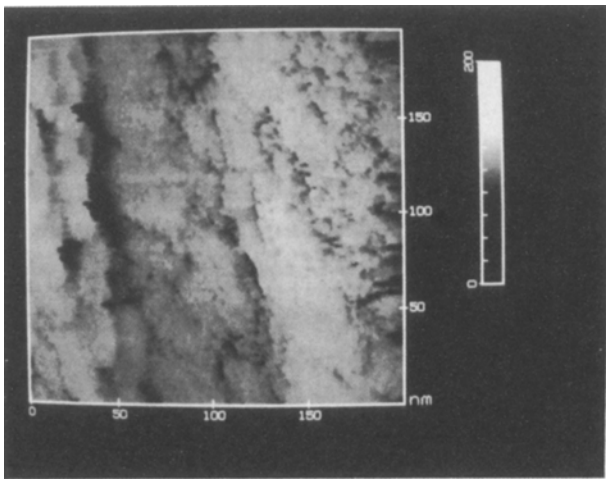

Figure 9 A higher magnification (200 nm scan) view of the unoxidized unsized celion fibre in Fig. 8 showing a disordered region.

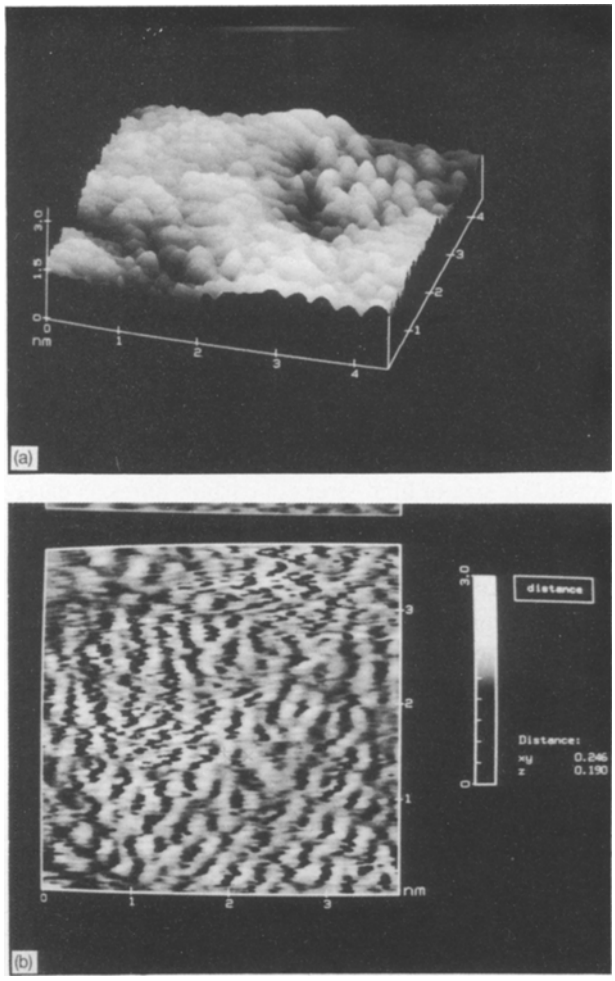

Figure 10 (a) A surface view of an unoxidized unsized Celion fibre showing atomic detail. (b) A top view of a 35 × 35 nm area of a Celion (uu) fibre showing limited graphitic structure. (Note the atomic separation of 0.246 nm).

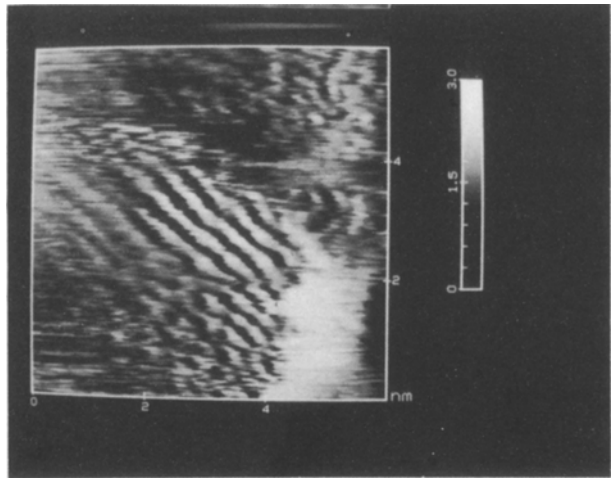

Figure 11 A 30 nm top view scan of a Celion (uu) fibre surface containing an area where the basal planes are oriented perpendicularly to the fibre surface.

demonstrates that there are the beginnings of graphitic order. On these low-temperature fibres it is even possible to find small areas of rather well-ordered material (Fig. 11) at the fibre surface. However, these small-ordered areas are usually surrounded by less-ordered material.

The parallel lines of atoms in the centre of Fig. 11 are separated by a distance which nearly corresponds to the interlayer distance of the graphite crystal (0.3354 nm). This means that this micrograph contains a small crystallite with the layer edges of the graphite crystal oriented perpendicularly to the fibre surface. The crystallite height, L_c, of the carbon layers in this relatively perfect crystallite (four lines) amounts to about 1 nm. This distance corresponds to the mean crystallite size of high-strength carbon fibres as determined by Guigon *et al.* with the aid of selected-area-electron-diffraction measurements [9].

Layers oriented perpendicular to the fibre surface are very important for the formation of functional surface groups, which are again important for the adhesion of polymer matrices. However, to avoid giving the wrong impression, it should be mentioned here that crystallites oriented perpendicularly to the surface are not at all common. In the vast majority of the micrographs, the basal planes of the crystallites are almost always parallel or nearly parallel to the surface.

In general it may be concluded from the few representative micrographs shown above that the surface exhibits not only a microroughness but even a nanoroughness. Also, it is apparent that the surfaces of these fibres do not contain a great deal of order. Thus, the bonding to these fibre surfaces takes place not on graphitic edge sites but on active sites that result from the disorder and roughness of the surface.

3.2.1.2. Industrially oxidized fibres (ou). Scanning tunnelling micrographs of the surfaces of fibres industrially oxidized by an undisclosed proprietary treatment are shown in Figs 12 and 13.

Investigations with the same Celion fibre discussed above but after commercial oxidation showed that the structure of the unoxidized fibre principally still remains. However, the microholes are enlarged and more interconnected (Fig. 12).

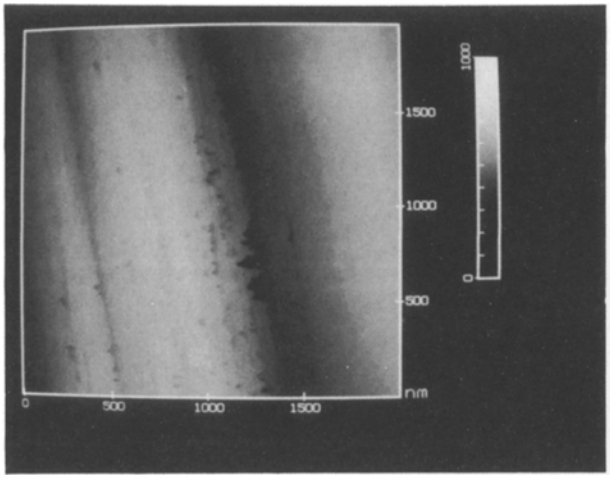

Figure 12 A 2 μm scan on a Celion (ou) fibre surface showing fibrils oriented along the fibre axis and some pitting.

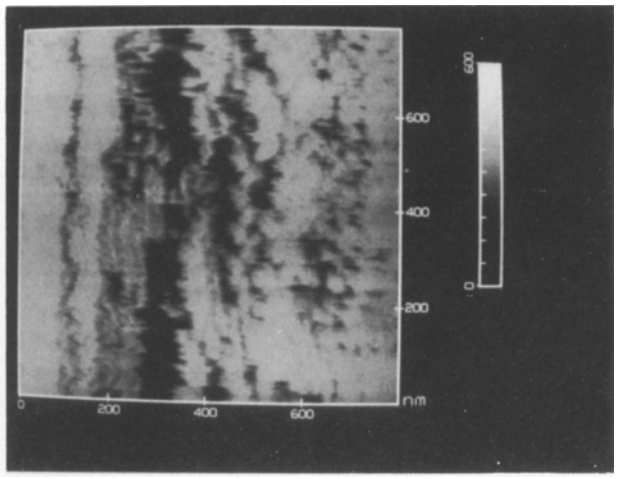

Figure 14 An 800 nm scan showing augmentation in pitting of the Celion (uu) fibre surface resulting from ozone treatment.

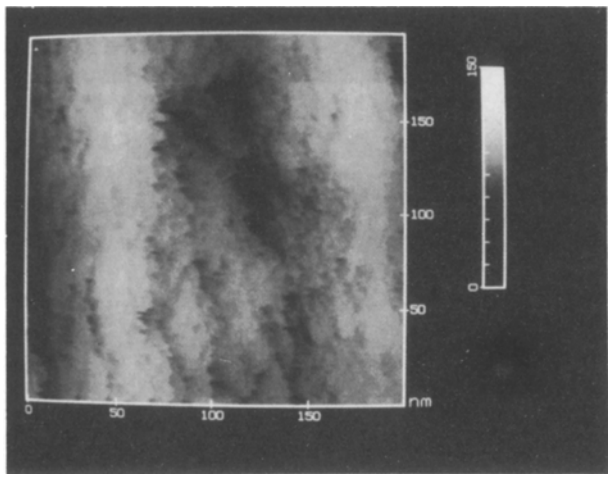

Figure 13 A higher-magnification view (200 nm scan) of the Celion (ou) fibre surface in Fig. 12 showing the surface and a pit.

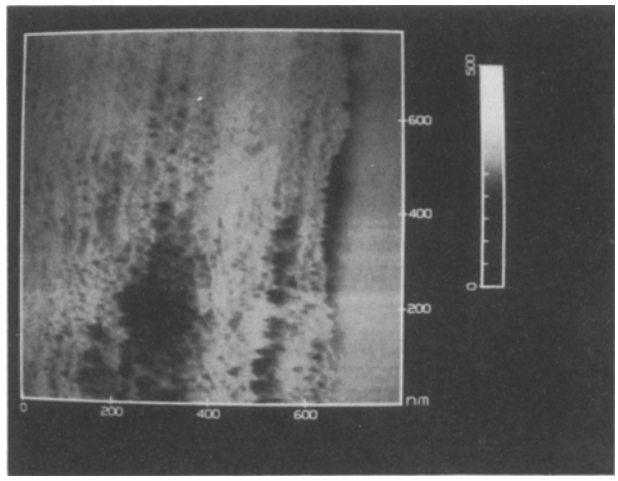

Figure 15 An 800 nm scan of an ozone-treated Celion (uu) fibre surface depicting pitting that resulted in a relatively ordered area on the surface.

Fig. 13 shows a scanning tunnelling micrograph of the same fibre but at higher magnification. These fibres have the same atomic structure as the unoxidized fibres. The main difference from the unoxidized fibre is in the increase in roughness which can be at all magnifications; this makes it difficult to image these fibres by STM. Also, these fibres do not appear to be uniformly oxidized. That is, some fibres exposed to the oxidation treatment appear smooth while others are significantly roughened. This is possibly due to either the non-uniform oxidation throughout the fibre bundle or to the lack of significant defects in some fibres. The current data points to the fact that both of these possibilities play a part.

3.2.1.3. Ozone-treated fibres. The ozone treatment of fibre surfaces was investigated in a parametric study varying the concentration of ozone, the treatment time and temperature, and the flow rate. It was found that the optimal conditions were 0.75% ozone in 20 l h^{-1} oxygen for 60 s at 100 °C. The results of the STM studies on a fibre treated under these conditions are summarized in Figs 14 to 17. The impression from all the micrographs, independent of the magnification, is that in general the surface roughness of the ozone-treated fibres is tremendously increased in comparison to the unoxidized or to the industrially oxidized fibres. On the other hand, it should be stated that there are still some areas on the surface that look relatively smooth. From a detailed analysis of the micrographs it was concluded that the less-ordered areas of the surface are preferentially attacked by ozone. The holes are enlarged in all dimensions, resulting in some channels of significant width (up to 100 nm) and depth (> 400 nm). Additionally, the concentration of the holes was increased (Fig. 14) as new holes were formed in previously smooth regions (Fig. 15). This leads to additional surface roughness. This kind of surface roughness is formed by a high concentration of small holes (width and length < 35 nm, depth < 50 nm). Deeper pores in these areas are less significant (Fig. 16), while larger pore entrances at the fibre surface are only rarely found (Fig. 17).

From the micrographs presented, it may be concluded that ozone in spite of its extreme reactivity primarily attacks the less-ordered ranges of the surface. In this regard, the activation with ozone is similar to an industrial-activation process. However, the attack of the surface during the ozone treatment is much more vigorous than during an industrial-oxidation process. From these observations it may be deduced that industrial oxidation is a rather mild process, probably chosen for minimal fibre damage. However, we have measured the strength of the ozone-treated fibres and obtained the same values as those measured before the treatment, which indicates that there is no significant fibre damage with this process. Therefore, it can be concluded that the ozone treatment is very effective in producing an enhanced surface roughness resulting in an increase in the number of sites which can interact with the matrix without affecting the mechanical properties of the fibres.

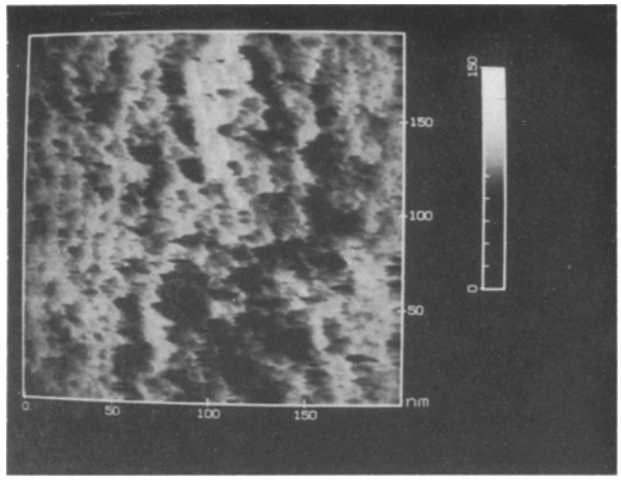

Figure 16 The increase in surface roughness resulting from ozone treatment on a Celion (uu) fibre surface is evident at all magnifications.

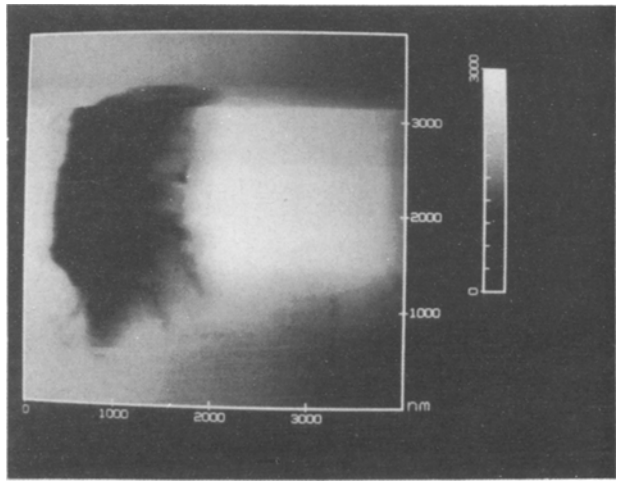

Figure 17 A 4 μm scan on a Celion (uu) fibre surface revealing a large pore, presumably caused by ozone treatment.

3.2.1.4. Oxygen-treated fibres. Figs 18–20 present scanning tunnelling micrographs of the Celion fibres after oxidation at 400 °C in pure oxygen for 30 min. All the micrographs display significant changes in the fibre surface when compared to the unoxidized fibres.

Extended areas of the fibre surface have broad channels which are oriented parallel to the fibre axis. This is similar to the observations for pitch fibres [20] subjected to a similar oxidation process. The width of the channels at the surface is approximately 150 nm, while the depth reaches nearly 200 nm (Fig. 18).

Another typical structure resulting from oxygen treatment is shown in Fig. 19. Pores formed by oxidation in these fibres are rare. Instead of deep pores, shallow cavities and step-like structures, such as seen in Fig. 20, are produced.

A comparison between the oxygen-treated fibres and the ozone-treated fibres shows that, although there is not as much pitting, the surface roughness resulting from oxidation is greater than that resulting from the ozone treatment. However, it cannot clearly be concluded at this time whether this increased roughness results from an attack of more-ordered regions or not.

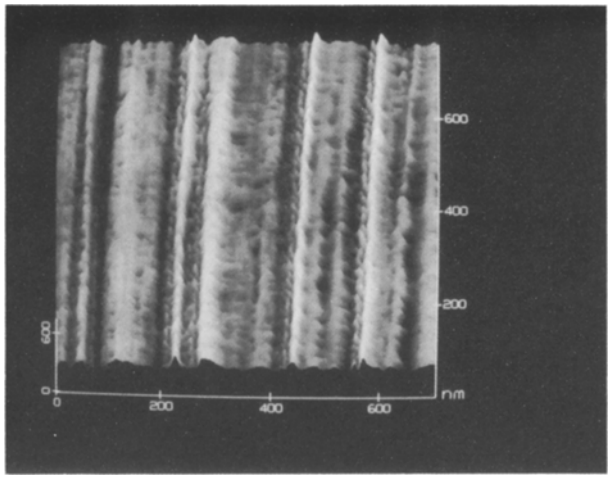

Figure 18 A 700 nm scan depicting the deep channels running along the fibre axis that resulted from treatment of a Celion (uu) fibre in oxygen at elevated temperatures.

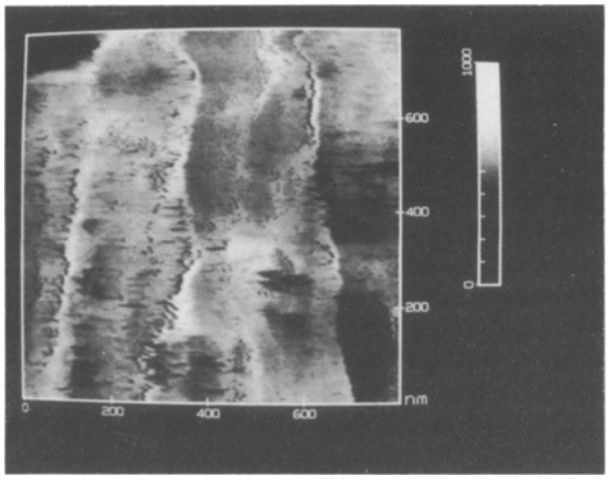

Figure 19 Large steps oriented along the fibre axis are also observed on Celion (uu) fibres exposed to oxygen at elevated temperature.

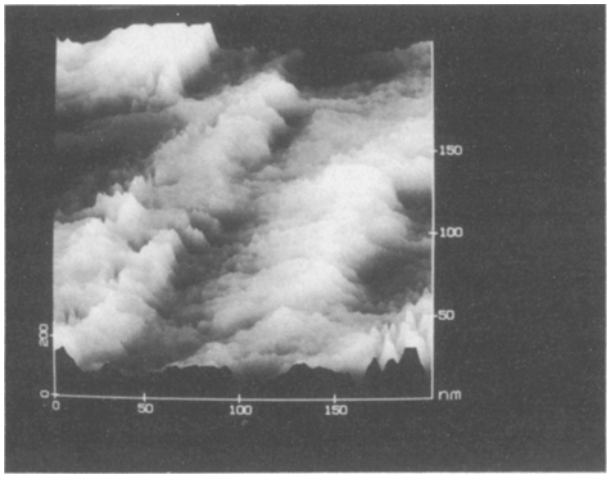

Figure 20 Small steps oriented nearly parallel to the fibre axis are also observed on a Celion (uu) fibre treated in oxygen at 400 °C.

3.2.2. Tenax-type fibres

3.2.2.1 Unoxidized fibres. Like the Celion fibres, Tenax carbon fibres also use PAN as a precursor. For this reason, it was interesting to determine if significant differences exist between the surface morphologies or structures of the Tenax and the Celion fibres.

At all magnifications, the unoxidized Tenax fibres were the smoothest of the fibres used in this study. Scanning tunnelling micrographs of this fibre are shown in Figs 21 and 22. Fig. 21 shows both relatively ordered and less-ordered regions with the less-ordered regions exhibiting small holes. The holes appear to be more random and uniformly distributed than on the surface of the unoxidized Celion fibres (Fig. 8). Additionally, the fibre surface seems to be a little smoother and the holes along the fibre axis are a little smaller. Nevertheless, a similarity between the surface morphology of the Tenax and the Celion fibres is apparent.

Fig. 22 shows a small very smooth area of the Tenax fibre with atomic resolution. Although the structure is not perfectly graphitic because of the low heat-treatment temperature of the fibre, there is some graphitic character. The trigonally symmetric graphite structure which can be seen in parts of Fig. 22 is the structure which is most frequently observed on carbon-fibre surfaces [18, 20]. It can be seen that the atoms are

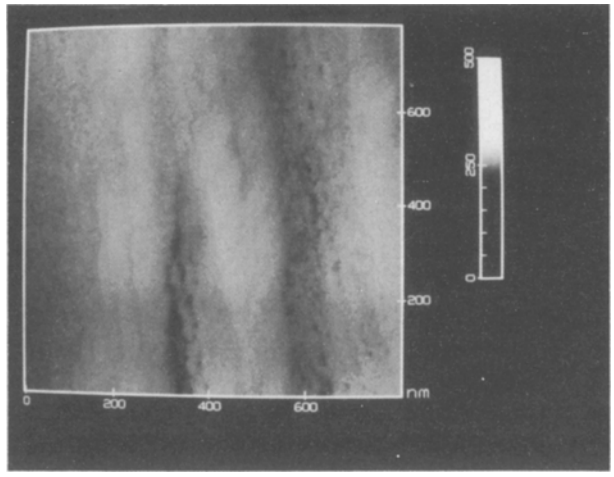

Figure 21 An 800 nm scan on a Tenax (uu) fibre surface shows that there are rather smooth regions as well as pitted areas.

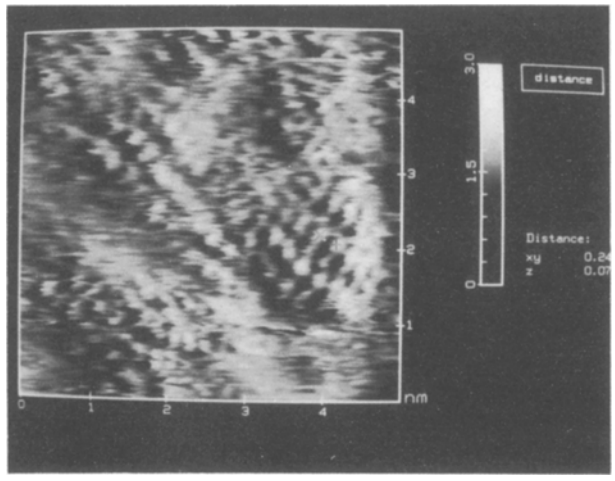

Figure 22 A 5 nm scan of a Tenax (uu) fibre surface showing graphitic structure with an atomic separation of 0.246 nm.

nearly regularly ordered with the smallest distance between two atoms being 0.246 nm. This interatomic distance is greater than the distance (0.142 nm) between two nearest neighbour atoms within a graphitic layer. The reason is that usually only every other atom in a graphitic layer can be imaged by STM. An explanation for this observation was given by Soler *et al.* [87] and it results from the difference in the electronic density of states in neighbouring atoms, which in turn results from the AB stacking in hexagonal graphite.

3.2.2.2. Industrially oxidized fibres. The results from the commercially oxidized Tenax fibre surfaces are shown in the micrographs of Figs 23–26. The micrographs show that there are rather smooth regions with less defects (Figs 23 and 24) as well as regions with significant cracks and pitting (Figs 25 and 26). In the micrographs at lower magnification, a fibrillar structure can be clearly observed. As with the other fibre types, there is an increase in the roughness of the commercially oxidized fibres compared to the unoxidized fibres. It appears from Figs 23 and 24 that the regions of higher order of the unoxidized fibres are only slightly attacked by the oxidation treatment.

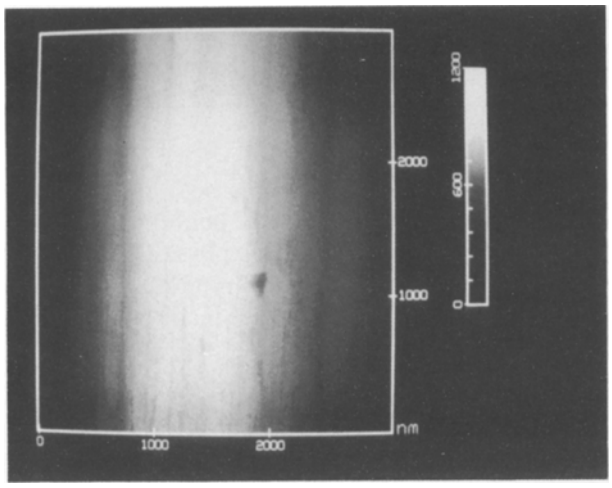

Figure 23 A 3 μm scan of a commercially surface-treated Tenax (ou) fibre; well-ordered and pitted areas are visible.

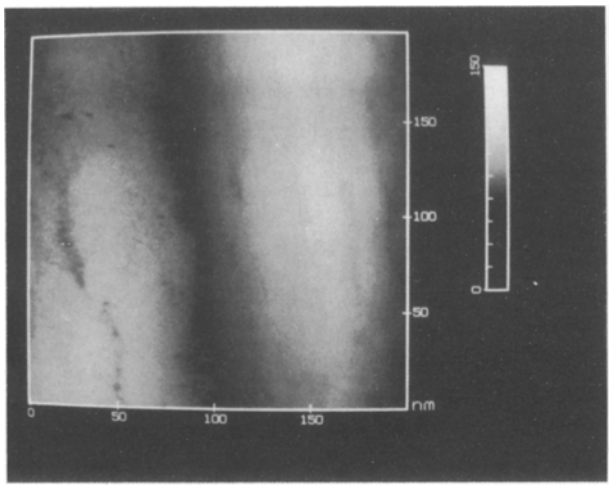

Figure 24 A higher-magnification (200 nm) scan showing a rather-well-ordered region of a commercially oxidized Tenax (ou) fibre surface.

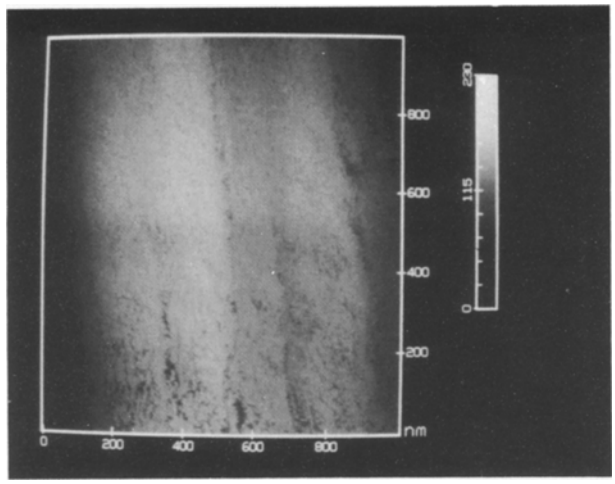

Figure 25 Less-ordered regions on the Tenax (ou) fibre surface.

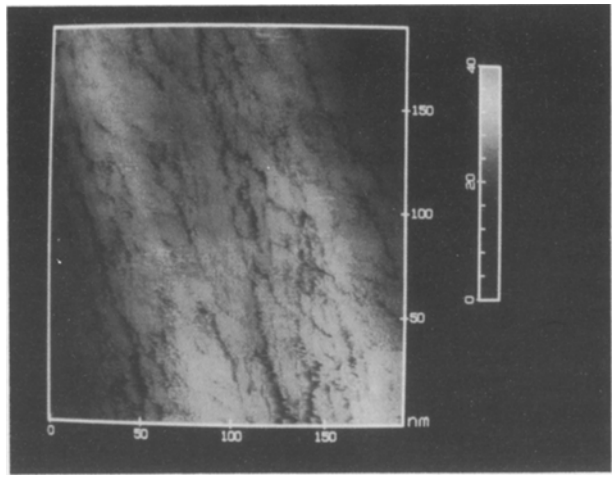

Figure 26 The texture of a disordered region on the commercially surface-treated Tenax (ou) fibre surface at higher magnification (a 200 nm scan).

Figs 25 and 26 show less-ordered areas of the oxidized fibre surfaces. Elongated holes with irregular shapes can be seen. These holes are arranged parallel to the axis and thus to the extrusion direction. At atomic dimensions in the smooth areas, no significant changes with the surface treatment were observed.

In comparison of the commercially oxidized Tenax fibres to the commercially oxidized Celion fibres, no significant differences in the structure and the surface roughness were observed. On the other hand, the roughening of the Tenax fibres as a consequence of the oxidation process is greater than that of the Celion fibres. Thus, although the Tenax fibres were smoother before oxidation, they were rougher after the oxidation process.

3.2.3. AS4 fibre

AS4 fibres are also based on PAN but were only available with industrial oxidation. Scanning tunnelling micrographs are shown in Figs 27–29. The

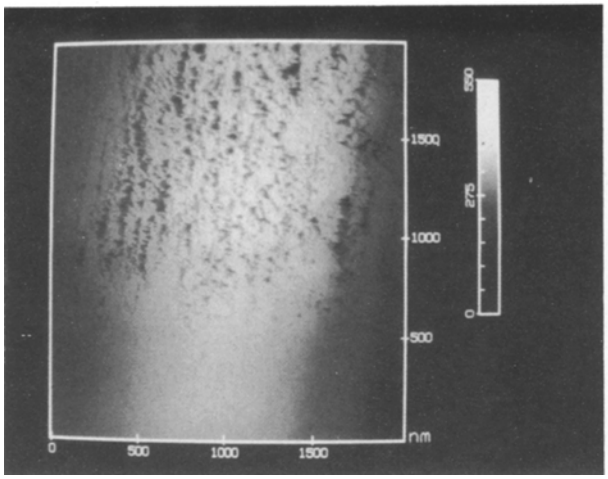

Figure 27 The AS4 (ou) surface on a micrometre scale like the other PAN fibres, has ordered and disordered areas.

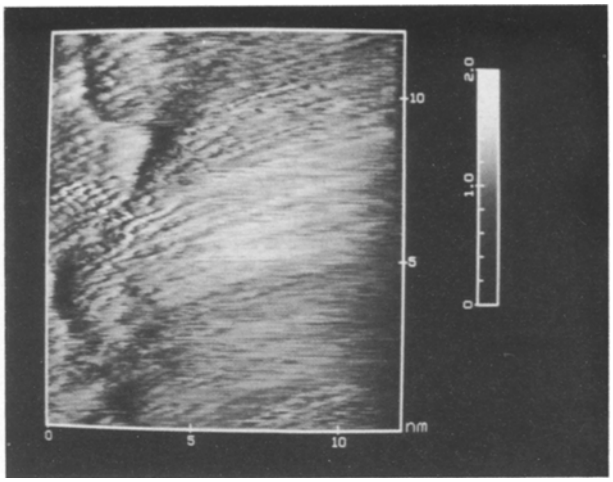

Figure 29 A 12 nm scan showing atomic structure superimposed on step-like structure.

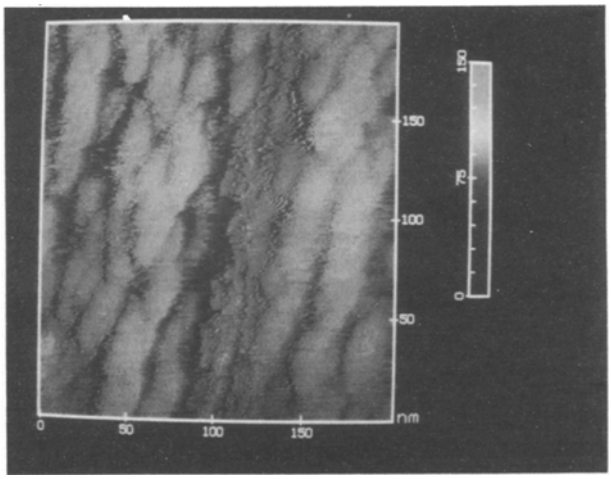

Figure 28 A higher magnification (200 nm) scan showing the surface texture of the AS4 (ou) fibre surface.

scanning electron micrographs have shown already that the surface structure of these fibres is significantly different from Celion or Tenax fibres. The AS4 fibre lacks a fibrillar structure and appears more homogenous. The preferred orientation of the surface structure parallel to the fibre axis is only slightly evident at this magnification (in Fig. 27). Coexistence of better and less-ordered areas (holes in rows) cannot be seen. Similar to the previous fibres, the surface is covered with numerous smaller and larger holes which, however, are shallow and more irregularly distributed across the surface (Figs 27 and 28).

At high magnification the surface reveals a stepwise rather than a nodular-type structure with atomic details. (Fig. 29). In this study, this structure was only seen on the surfaces of the surface-treated Celion fibre and this AS4 fibre. However, this structure is typical of PAN fibres, and it has been observed in other types of PAN fibres [88].

3.3. Adsorption studies

In an attempt to determine the total surface area, the active-surface-area, and the pore-volume distribution of the fibres used in this study, both physical and chemical adsorption studies were performed. Because the total surface area is so small, physical adsorption measurements were made using krypton at − 195 °C. Active surface measurements were made by chemisorbing oxygen at 300 °C.

TABLE III Active surface areas of various samples

Sample	Active surface area ($m^2 g^{-1}$)
Celion G-30-500 uu	0.029
Celion G-30-500-uu-O_3-100 °C	0.043
Celion G-30-500-uu-O_2-400 °C	1.331
Tenax HTA-uu	0.031
Tenax HTA-ou	0.053

Due, possibly, to the low processing temperature of these fibres, the adsorption studies were much less than fully successful. Because of outgassing from the fibre, which continued even after weeks of evacuation, it was not possible to determine the equilibrium amount of krypton physically adsorbed and thus the total surface area. However, the chemisorption studies were more successful. After outgassing the fibre for several days at 950 °C, it was possible to make reproducible measurements on the extent of oxygen chemisorption. It should be noted, however, that because of the long high-temperature outgassing some of the surfaces could have changed before the first active-surface-area measurement. Coupled with the fact that some of the values changed after the first active-surface-area measurement (but not between the second and third), the active-surface-area measurements can only be considered to be qualitative and useful for comparison only. Since all the adsorption runs took an inordinate amount of time, only fibres selected on the basis of the STM and preliminary adhesion results were studied. The results of these selected fibres are given in Table III.

It can be seen that with oxidation in both molecular oxygen and ozone there is a measurable increase in the active-surface-area that parallels the increase in the surface roughness. The various surface treatments ob-

viously produce significant differences in the fibre surface structure as well as in the roughness. However, as will be shown in Part III, the differences in surface roughness, as seen by STM, do not have a great effect on the adhesion to the matrix materials studied when measured by the interlaminar-shear strength. *A priori* one would not assume this, because friction and/or mechanical interlocking account for a significant part of the adhesion at the interface. The fact that the observed difference in roughness does not have a measurable effect on adhesion is a significant result, because for the first time a correlation has been made between the fibre surface roughness on the nanoscale and the composite properties. By observing the roughness on the nanometre scale, it has been possible to separate the effects of the roughness from the surface-chemistry effects as will be shown in Part III.

4. Conclusion

It is apparent from this study as well as from previous works that each carbon fibre is unique in both its micrometre and nanometre structures. These structures play an important role in determining the number of active sites and thus in the potential bonding ability of these fibres. The ability to see the surfaces of these fibres finally allows one to correlate the mechanical properties of a bond to the surface roughness and to attempt to quantify the contribution. The relative influence of the surface roughness and the degree of bonding on the mechanical properties of composites formed with the fibres used in this study will be addressed in Part III in this series.

Acknowledgement

The financial support of this study by the German Research Foundation (DFG) is gratefully acknowledged.

References

1. A. F. TURBAK and T. L. VIGO in "High-tech fibrous materials", edited by A. F. Turbak, T. L. Vigo, ACS Symposium Series (American Chemical Society, Washington DC, 1991) 1.
2. E. FITZER, *Carbon* **27** (1989) 621.
3. K. J. HUTTINGER in "Haftung in verbundstoffen und verbundwerkstoffen", edited by W. Brockmann (DGM-Informationsgesellschaft, 1990) p. 221.
4. *Idem., High temp.-high pressure* **22** (1990) 317.
5. *Idem.*, in "Carbon fibres, filaments and composites", edited by J. L. Figueiredo *et al.*, (Kluwer Academic, Dordrecht, 1990) p. 245.
6. E. FITZER and M. HEYM, *Chem. Indust.* **1** (1976) 663.
7. H. D. BODER, D. GOLDEN, P. ROSE and M. WURMSEHER, *Z. Werkstofftech.* **11** (1980) 275.
8. J. D. H. HUGHES, *J. Phys. D* **20** (1987) 276.
9. M. GUIGON, A. OBERLIN and G. DESARMOT, *Fibre Sci. Tech.* **20** (1984) 565.
10. M. ENDO, *J. Mater. Sci.* **23** (1988) 598.
11. W. FROHS, E. FITZER and F. ROZPLOCH, *High Temp.-High Pressure ETPC Proc. 10* **19** (1987) 311.
12. A. OBERLIN, *Carbon* **17** (1979) 7.
13. S. C. BENNETT and D. J. JOHNSON, *ibid.* **17** (1979) 25.
14. D. J. JOHNSON, *Chem. Indust.* **22** (1982) 692.
15. C. T. HERAKOWITCH, *Carbon* **27** (1989) 663.
16. J. B. DONNET and A. VOET, "Carbon Black," (Marcel Dekker, New York, 1976) p.106.
17. K. J. HUTTINGER, *Chemiker-Zeitung* **112** (1988) 335.
18. W. P. HOFFMAN, W. C. HURLEY, P. M. LIU and T. W. OWENS, *J. Mater. Res.* **6** (1991) 1685.
19. W. P. HOFFMAN, V. B. ELINGS and J. A. GURLEY, *Carbon* **26** (1988) 754.
20. W. P. HOFFMAN, W. C. HURLEY, T. W. OWENS and H. T. PHAN, *J. Mater. Sci.* **26** (1991) 4545.
21. H. P. BOEHM and G. BEWER, Extended Abstracts of the Fourth London International Carbon and Graphite Conference (1974) 344.
22. H. P. BOEHM, E. DIEHL, W. HECK and R. SAPPOCK, *Angew. Chem.* **76** (1964) 742.
23. H. P. BOEHM, *Kolloid Z. Z. Polym.* **227** (1968) 17.
24. *Idem., Adv. Catalysis* **16** (1966) 179.
25. H. P. BOEHM and M. VOL, *Carbon* **8** (1970) 227; *Idem., ibid.* **8** (1970) 741; *Idem., ibid.* **9** (1971) 473; and *Idem., ibid.* **9** (1971) 481.
26. J. B. DONNET and R. C. BANSAL, "Carbon fibres", (Marcel Dekker, New York, 1984).
27. P. EHRBURGER in "Carbon fibres, filaments and composites", J. L. Figueiredo *et al.* (Eds.), (Kluwer Academic Publishers, Dordrecht, 1990) 147.
28. D. W. McKEE and V. J. MIMEAULT in *Chem Phys Carbon* **8** (1973) 151.
29. B. R. PURI in *ibid.* **6** (1971) 191.
30. G. BREWER, PhD dissertation, University of Munich, Munich, (1975).
31. J. H. BLOCK, A. M. BRADSHAW, P. C. GRAVELLE, J. HABER, R. S. HANSEN, M. W. ROBERTS, N. SHEPPARD and K. TAMARU, *Pure & Appl. Chem.* **62** (1990) 2297.
32. P. DENISON, F. R. JONES and J. F. WATTS, *J. Phys. D* **20** (1987) 306.
33. Y. NAKAYAMA, F. SOEDA and A. ISHITANI, *Carbon* **28** (1990) 21.
34. A. PROCTOR and P. M. A. SHERWOOD, *J. Electron Spectrosc. Related Phenom.* **27** (1982) 39.
35. *Idem., Carbon* **21** (1983) 53.
36. A. PROCTOR and P. M. A. SHERWOOD, *Surface Interface Analysis* **4** (1982) 212.
37. C. KOZLOWSKI, and P. M. A. SHERWOOD, *J. Chem. Soc., Faraday Trans. I* **80** (1984) 2099, and *Idem., ibid.* **81** (1985) 2745.
38. *Idem., Carbon* **25** (1987) 751.
39. F. HOPFGARTEN, Extended Abstracts of the thirteenth Biennial Conference on Carbon, edited by C. A. Irvine (1977) 288.
40. J. ZAWADZKI in "Chemistry and Physics of Carbon", edited by P. A. Thrower, Volume 21 (Marcel Dekker, New York, 1989) 147.
41. C. SELLITTI, J. L. KOENIG and H. ISHIDA, *Carbon* **28** (1990) 221.
42. V. A. GARTEN and D. E. WEISS, *Rev. Pure & Appl. Chem.* **7** (1957) 69.
43. *Idem., Aust. J. Chem.* **10** (1959) 309.
44. K. KONISHITA, "Electro-chemical and physico-chemical properties of carbon" (Wiley, New York, 1988).
45. H. P. BOEHM, *Angew. Chemie* **78** (1966) 717.
46. E. PAPIRER, J. DENTZER, S. LI and J. B. DONNET, *Carbon* **29** (1991) 69.
47. S. S. BARTON and B. H. HARRISON, *ibid.* **13** (1975) 283.
48. B. R. PURI and R. C. BANSAL, *ibid.* **1** (1964) 451, and *Idem., ibid.* **1** (1964) 457.
49. G. TREMBLAY, F. J. VASTOLA and P. L. WALKER Jr, *ibid.* **16** (1978) 35.
50. D. RIVIN, *Rubber Chem. Tech.* **36** (1963) 729, and *Idem., ibid.* **44** (1971) 307.
51. F. M. FOWKES in "Physico-chemical aspects of polymer surfaces", Vol. 2 (Plenum Press, New York, 1983) 583.
52. *Idem., J. Adhesion Sci. Tech.* **1** (1987) 7.
53. W. A. ZISMAN in "Contact angle, wettability, and adhesion" edited by R. F. Could, ACS Advanced Chemistry Series 43 (American Chemical Society, Washington DC. 1964) p. 1.
54. S. ROSS and J. D. MORRISON, "Colloid systems and interfaces" (Wiley, New York, 1988) 99.

55. A. W. NEUMANN and R. J. GOOD in "Surface and colloid science", edited by R. J. Good and R. R. Stromberg, (Plenum Press, New York, 1979) 31.
56. W. C. BIGELOW, D. L. PICKETT and W. A. ZISMAN, *J. Coll. Sci.* **1** (1946) 513.
57. Y. TAMAI, K. MAKUUCHI and M. SUZUKI, *J. Phys. Chem.* **71** (1967) 4176.
58. J. SCHULTZ, K. TSUTSUMI and J. B. DONNET, *J. Coll. Interf. Sci.* **59** (1977) 272.
59. W. C. HAMILTON, *ibid.* **40** (1971) 219.
60. *Idem., ibid.*, **47** (1974) 672.
61. S. HOHMANN-WIEN, PhD dissertation, University of Karlsruhe (1991).
62. K. J. HUTTINGER, S. HOHMANN-WIEN and M. SEIFERLING, *Carbon* **29** (1991) 449.
63. K. J. HUTTINGER, S. HOHMANN-WIEN and G. KREKEL, *ibid.*, **29** (1991) 1281.
64. *Idem. J. Adhesion Sci. Tech.* **6** (1992) 317.
65. C. S. BROOKS and D. A. SCOLA, *J. Coll. Interf. Sci.* **32** (1970) 561.
66. J. R. CONDER and C. L. YOUNG, "Physico-chemical applications of gas chromatography", (Wiley-Interscience, New York, 1979).
67. J. SCHULTZ, C. LAVIELLE and C. MARTIN, *J. Adhesion* **23** (1987) 45.
68. G. M. DORIS and D. G. GRAY, *J. Coll. Interf. Sci.* **71** (1979) 93.
69. E. PAPIRER, H. BALARD and A. VIDAL, *Eur. Polym. J.* **24** (1980) 783.
70. J. B. DONNET and P. EHRBURGER, *Carbon* **15** (1977) 143.
71. L. T. DRZAL, J. M. RICH and P. F. LLOYD, *J. Adhesion* **16** (1982) 1.
72. L. T. DRZAL, J. M. RICH, F. M. KOENIG and P. F. LLOYD, *ibid.* **17** (1983) 133.
73. K. H. GEIGL, PhD dissertation, University of Karlsruhe (1980).
74. E. FITZER, K. H. GEIGL, W. HUTTNER and R. WEISS, *Carbon* **18** (1980) 389.
75. R. WEISS, PhD dissertation, University of Karlsruhe (1984).
76. E. FITZER and R. WEISS, *Carbon* **25** (1987) 455.
77. H. JAGER, PhD dissertation, University of Karlsruhe (1986).
78. H. P. RENSCH, PhD dissertation, University of Karlsruhe (1990).
79. E. FITZER, N. POPOVSKA, H. P. RENSCH, *J. Adhesion* **36** (1991) 139.
80. P. EHRBURGER, J. J. HERQUE, J. B. DONNET, *London, Soc. Chem. Ind.* **1** (1978) 398.
81. R. WEISS, Proceeding Verbundwerk, Wiesbaden, Demat (1988).
82. H. KELLER, Proc. of the second Symposium Materialforschung, Dresden, BMFT, 1 (1991) p. 48.
83. F. ORTH, G. W. EHRENSTEIN, Proceedings of the second Symposium Materialforschung, Dresden, BMFT, 2 (1991) 1307.
84. N. R. LAINE, F. J. VASTOLA, and P. L. WALKER Jr, *J. Phys. Chem.* **67** (1963) 2030.
85. W. P. HOFFMAN and J. A. LOWRY, in Extended Abstracts 16th Biennial Conference on Carbon, San Diego, June 1983, p. 357.
86. S. BRUNAUER, P. H. EMMETT and E. J. TELLER, *Amer. Chem. Soc.* **60** (1938) 309.
87. J. SOLER, A. M. BARO, N. GARCIA, H. ROHRER, *Phys. Rev. Lett.* **57** (1986) 444.
88. W. P. HOFFMAN, *Carbon* **30** (1992) 315.

Received 5 April
and accepted 8 October 1993